Temperature Effects on the Electrochemical Behavior of Spinel $LiMn_2O_4$ in Quaternary Ammonium-Based Ionic Liquid Electrolyte

Honghe Zheng,*,†,‡ Hucheng Zhang,† Yanbao Fu,‡ Takeshi Abe,‡ and Zempachi Ogumi‡

College of Chemistry and Environmental Sciences, Henan Normal University, Xinxiang, 453007, People's Republic of China, and Department of Energy and Hydrocarbon Chemistry, Graduate School of Engineering, Kyoto University, Katsura Campus Nishikyo-ku, Kyoto 615-8510, Japan

Received: March 10, 2005; In Final Form: May 9, 2005

Temperature dependence of the physiochemical characteristics of a room-temperature ionic liquid consisting of trimethylhexylammonium (TMHA) cation and bis(trifluoromethane) sulfonylimide (TFSI) anion containing different concentrations of LiTFSI salt was examined. Electrochemical properties of a spinel $LiMn_2O_4$ electrode in 1 M LiTFSI/TMHA-TFSI ionic electrolyte were investigated at different temperatures by using cyclic voltammetry, galvanostatic measurements, and electrochemical impedance spectroscopy. The Li/ionic electrolyte/$LiMn_2O_4$ cell exhibited satisfactory electrochemical properties with a discharge capacity of 108.2 mA h/g and 91.4% coulombic efficiency in the first cycle under room temperature. At decreased temperature, reversible capacity of the cell could not attain a satisfactory value due to the high internal resistance of the cell and the large activation energy for lithium ion transfer through the electrode/electrolyte interface. Anodic electrolyte oxidation results in the decrease of coulombic efficiency with increasing temperature. Irreversible structural conversion of the spinel $LiMn_2O_4$ in the ionic electrolyte, possibly associated with the formation of TMHA intercalated compounds and/or Jahn−Teller distortion, was considered to be responsible for the electrochemical decay with increasing cycles.

I. Introduction

With advantages of nonflammability, high thermal and chemical stability especially toward moisture, wide liquid-phase range, negligible vapor pressure, high conductivity, and easy recycling, room-temperature ionic liquids (RTILs) are known as green solvents.[1−5] The new functional liquid materials, often offering some unique properties, are revolutionizing many fields of scientific and technological interest. Possible application of RTILs into different energy storage devices such as electric double layer capacitor[6,7] and solar cells[8,9] has been recently attracting considerable interest. RTILs are also finding potential use in lithium (ion) batteries so as to completely solve the safety problems and possibly widen the operating temperature range for electric vehicles or other large-scale power systems.[10−15] However, limitations such as high viscosity and poor wettability with active electrode materials restrict the successful use of ionic liquids into lithium ion batteries. In this sense, lots of fundamental studies have to be carried out before a satisfactory solution is found.

Since Wilkes[16] first demonstrated the stability of 1-ethyl-3-methylimidazolium tetrafluoroborate ((EMI)BF_4) toward moisture, studies dealing with the use of ionic liquids based on the EMI cations for advanced electrochemical devices have been focused due to their high ionic conductivity (up to 10^{-2} S cm^{-1}) and low viscosity properties. A Li−Al/$LiCoO_2$ battery using a 1-methyl-3-ethylimidazolium chloride room-temperature molten salt with the addition of 0.05 mol/kg $C_6H_5SO_2Cl$ showed satisfactory results with a discharging capacity of 112 mA h/g and better than 90% coulombic efficiency.[17] Nakagawa et al.[18] examined the electrochemical properties of a $LiCoO_2$ electrode in $LiBF_4$/(EMI)BF_4 ionic electrolyte with $Li_4Ti_5O_{12}$ as the counter electrode. A discharge capacity of the $LiCoO_2$ electrode was obtained to be around 120 mA h/g with 71.4% coulombic efficiency in the first cycle. Most recently, Garcia et al.[19] presented a lithium-ion cell using $LiCoO_2$ and $Li_4Ti_5O_{12}$ as the electrode materials with EMI−TFSI ionic electrolyte. $LiCoO_2$ cathode retained a reversible capacity of 106 mA h/g after 200 cycles. When $LiMn_2O_4$ cathode was cycled in an ionic electrolyte of LiCl saturated $AlCl_3$−EMIC melt, the electrode exhibited electrochemical behavior similar to that in conventional nonaqueous electrolytes.[20] For all the satisfactory experimental results obtained by different researchers, practical application of EMI-based ionic liquids as electrolyte for lithium ion batteries still seems difficult. The greatest difficulty in applying the ionic electrolyte comes from its narrow electrochemical windows (ca 4.2 V). Lithium ion batteries using EMI-based ionic liquids suffer from a relatively small operating voltage of about 3.0 V. Meanwhile, low cathodic stability of the electrolyte toward lithium metal[12,21] is another problem waiting solution.

Ionic liquids with more stable cations such as tetraalkylammonium, pyrrolidinium, and piperidinium cations show wider electrochemical windows and satisfactory cathodic stability toward lithium metal. Application of these ionic liquids into lithium ion batteries has shown better prospects.[22,23] The electrochemical properties of electrode materials in electrolytes based on ionic electrolyte systems have been preliminarily reported, and some of the results seem to be satisfactory. Sakaebe and Matsumoto[24] investigated the electrochemical properties of a $LiCoO_2$ cathode in ionic electrolytes consisting of various quaternary ammonium cations and imide anions.

* Corresponding author. Telephone.: +86-373-3326544. Fax: +86-373-3326544. E-mail: hhzheng66@yahoo.com.cn.
† Henan Normal University.
‡ Kyoto University.

10.1021/jp051238i CCC: $30.25
Published on Web 06/25/2005

N-Methyl-*N*-propylpiperidinium bis(trifluoromethanesulfonyl)-imide (PP13-TFSI) was found to be a promising candidate. Most recently, a pyrrolidinium-based ionic liquid electrolyte and a room-temperature ionic liquid consisting of *N*,*N*,*N*,*N*-cyanomethyl trimethylammonium (CTMA) cation and bis(trifluoromethanesulfonyl)imide (TFSI) anion were synthesized.[25,26] Both the two ionic liquids demonstrated an improved lithium deposition/dissolution cycling behavior.

Although with excellent thermal stability and wide liquid-phase range, physiochemical properties of ionic liquids such as viscosity, conductivity, and density are strongly dependent on temperature.[27,28] Therefore, temperature will significantly influence the electrochemical performance of a lithium (ion) battery using electrolyte based on a room-temperature ionic liquid. However, temperature effects on the electrochemical behavior of a lithium (ion) battery using an ionic electrolyte have rarely been reported to the best of our knowledge.

In this study, a tetraalkylammonium ionic liquid is used as the battery electrolyte because it exhibits satisfactory cathodic stability toward lithium metal and seems promising for practical application into lithium (ion) batteries. The temperature effects on the physiochemical properties of a room-temperature ionic liquid consisting of trimethylhexylammonium (TMHA) cation and TFSI anion containing different concentrations of LiTFSI salt were addressed. The electrochemical behavior of a spinel $LiMn_2O_4$ electrode in 1 M LiTFSI/TMHA-TFSI ionic electrolyte was investigated under different temperatures. Possible mechanisms concerning the temperature effects on the electrochemical behavior of the spinel $LiMn_2O_4$ electrode in the ionic electrolyte were discussed.

II. Experimental Section

TMHA−TFSI was prepared according to the following procedure. Equal amounts of anhydrous LiTFSI and TMHABr were dissolved in purified water. Mixing the two solutions followed by vigorously stirring for several hours at 70 °C resulted in separation into a TMHA−TFSI and an aqueous phase. The TMHA−TFSI was extracted into CH_2Cl_2 and then thoroughly washed with purified water. The final product was obtained after vacuum evaporation and vacuum-drying at 100 °C overnight.[29] The water content of the TMHA−TFSI sample was determined to be less than 20 ppm. LiTFSI/TMHA−TFSI ionic electrolyte was prepared by dissolving different amounts of LiTFSI as supporting electrolyte.

Thermal analysis of 1 M LiTFSI/TMHA−TFSI ionic electrolyte was conducted by a differential scanning calorimeter (DSC) and thermal gravimetric analysis (TGA). DSC studies were performed on a Shimadzu DT-40 thermal analyzer. A sample weighing 5 mg was sealed in a flat-bottomed aluminum pan and quenched, initially to −110 °C for 30 min, and then heated with a heating rate of 5 °C/min. Thermogravimetric analysis was performed in an alumina (Al_2O_3) pan with a heating rate of 5 °C/min under N_2.

Electrolyte viscosities were determined by using a suspended-level Ubbelohde viscometer with a thermostatic oil bath. Flow time measurements are performed by a Schott AVS 310 photoelectric time unit with a resolution of 0.01 s. The viscometer was calibrated using the efflux time of purified water. Solution viscosity, η, is calculated by the following equation:

$$\rho/\eta = ct - k/t \quad (1)$$

where c and k are the viscometer constants and t is the efflux time. The experimental error of densities was determined to be $\pm 1 \times 10^{-5}$ g·cm^{-3} with an Anton Paar DMA 60/602 vibrating-tube digital densimeter with the same temperature precision as the viscosity measurements. The estimated error of experimental viscosity is ±0.5%. The details of the experimental procedure are given elsewhere.[30]

The electrolyte conductivity was measured by the ac impedance method in the frequency range of 10 MHz to 100 Hz, using a conductivity cell (cell constant = 1.02). The cell was calibrated with 0.1 M KCl solution. The temperature was controlled to be as precise as the viscosity measurements. The estimated error of experimental conductivity is ±1%.

Electrochemical windows of the neat TMHA−TFSI ionic liquid were measured by cyclic voltammetry. Cu foil, Ni foil, Al foil, glassy carbon, and actylene black were employed as the working electrode, respectively. Lithium foil was used as both counter and reference electrode. The electrode was polarized in the potential range of 0−5 V vs Li/Li$^+$ with a scan rate of 0.1 mV/s.

The $LiMn_2O_4$ electrode was prepared by mixing $LiMn_2O_4$ powder with binder (PVDF) and conductor (acetylene black) by a weight ratio of 85:5:10. Then the mixture was rolled onto Al foil and cut into pellets. The loading of active material was ca. 2 mg/cm^2. Three electrode cells were assembled in an argon-filled glovebox with the dew point below −80 °C. Lithium foil was used as counter and reference electrode, respectively. Cyclic voltammetry of the $LiMn_2O_4$ electrode in the ionic electrolyte was conducted over the potential range of 3.0−4.5 V with a scan rate of 0.05 mV/s. The constant current charge−discharge experiment was carried out with the current density of 15 mA/g. The operating voltage was set between 3.3 and 4.3 V.

Lithium ion transfer through the interface between the spinel $LiMn_2O_4$ electrode and the ionic electrolyte was measured with electrochemical impedance analysis using Sorlatron 1255. Considering a significant impedance at the lithium interface exists in this type of electrolyte, three electrode electrochemical cells were employed.[31] Prior to ac impedance measurements, the $LiMn_2O_4$ electrode was held at 3.94 V for at least 1 h to attain the condition of sufficiently low residual current. EIS was carried out by applying an ac amplitude of 5 mV over the frequency range of 100 kHz to 10 mHz.

The structure of the $LiMn_2O_4$ electrode before and after electrochemical cycles in different electrolytes was characterized by X-ray diffraction (XRD) with an automated Rigaku X-ray diffractometer using Cu Kα radiation. The diffraction angle (2θ) was measured between 30 and 70° with an increment of 1°/min.

III. Results and Discussion

3.1. Physiochemical Properties of the TMHA−TFSI Ionic Liquid Systems. The thermal behavior of the 1 M LiTFSI/TMHA−TFSI ionic electrolyte was determined by DSC and TGA. Figure 1a shows the DSC curves of the ionic electrolyte. The quenched sample showed two endothermic peaks on heating. The glass transition temperature (T_g) and melting point (T_m) were observed to be −65.2 and 14.1 °C, respectively. The DSC trace obtained here is quite in agreement with that reported by McFarlane et al.,[32] in which the glass transition point of the neat TMHA−TFSI was determined to be −74 °C. Considering the addition of 1 M Li salt may increase T_g to a certain degree,[18] this result is reliable. A clear exothermic peak at −7.7 °C is attributed to the cold crystallization of the electrolyte during the warming process.

Figure 1b shows the TGA curves of TMHA−TFSI containing 1 M LiTFSI from 25 to 500 °C. A 1 M amount of LiTFSI/TMHA−TFSI ionic electrolyte was stable up to 280 °C and

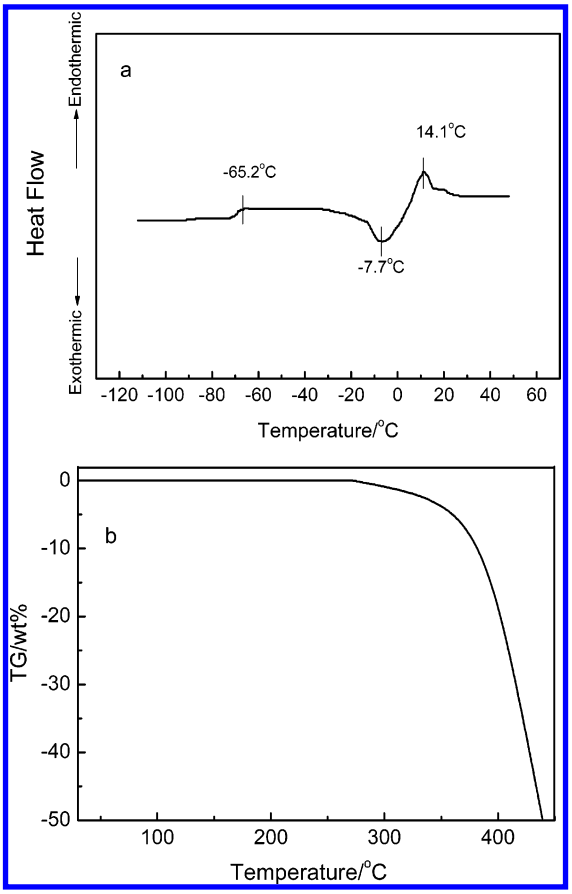

Figure 1. (a) DSC curve of TMHA−TFSI ionic liquid containing 1 M LiTFSI and (b) TGA curve of TMHA−TFSI ionic liquid containing 1 M LiTFSI.

decomposed rapidly over 350 °C. On the basis of this result, the ionic electrolyte is stable enough to be used as electrolytes for electrochemical devices over a wide range of temperature.

Density is a useful physical property of ionic liquids for battery application. However, many of the density values reported are at a single temperature, usually at 298.15 K. Experimental density data for the TMHA−TFSI ionic liquid containing different concentrations of LiTFSI salt (Figure 2) shows a linear dependence on temperature. A linear equation of the following form is confirmed:

$$\rho = a + bT \tag{2}$$

where ρ is the density, a is a constant referring to the sample density at an absolute temperature of 0 K, b is a constant referring to the variation rate of the sample density with temperature, and T is the absolute temperature. For pure TMHA−TFSI ionic liquid, a and b were obtained to be 1.4371 g·cm^{-3} and -3.021×10^{-4} g·cm^{-3}·K^{-1}, respectively, by linear regression with a correlation coefficient greater than 0.99. The constants a and b included in the equation slightly increase with increasing LiTFSI concentration. For TMHA−TFSI containing 1 M LiTFSI salt, a and b were obtained to be 1.5607 g·cm^{-3} and 4.271×10^{-4} g·cm^{-3}·K^{-1}, respectively. This equation is useful for predicting volume variations with the temperature of an electrolyte within a battery.[33]

Viscosity is an important physical property affecting diffusion of ions. Ionic liquid systems are known to be more viscous than traditional nonaqueous electrolyte. Figure 3a represents the variations of viscosity of TMHA−TFSI with LiTFSI concentrations under room temperature (30 °C). For pure TMHA−TFSI ionic liquid, its viscosity is determined to be 120.3 mPa·s. The viscosity measured in this study was close to the reported literature value.[32] With addition of LiTFSI salt, the electrolyte becomes more viscous and the TMHA−TFSI ionic solution becomes extremely viscous when dissolved 1 M LiTFSI salt.

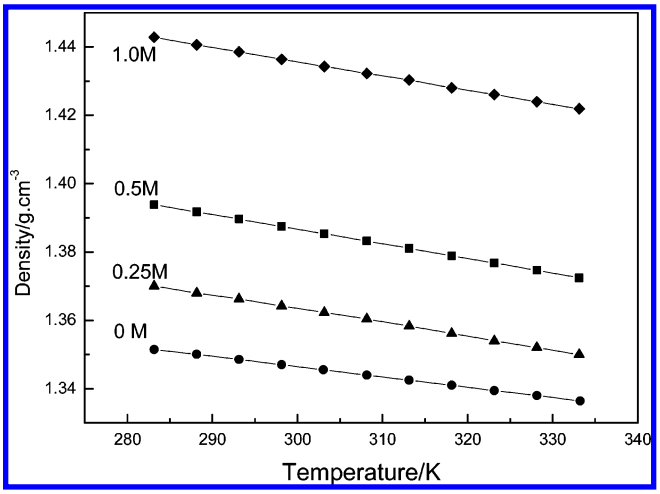

Figure 2. Variation of solution density with temperature for TMHA−TFSI ionic lquid containing differing concentrations of LiTFSI salt.

Viscosity temperature dependence is also very complicated compared with that of nonaqueous organic electrolyte.[34] The temperature dependence of viscosity was studied over the temperature range of 283−333 K. As shown in Figure 3b, the viscosity of the TMHA−TFSI solution increases as the temperature decreases with tendencies depending on the LiTFSI concentration. The higher the LiTFSI concentration is, the more rapidly the viscosity increases with decreasing temperature. There is about a 5-fold increase in the viscosity for the pure TMHA−TFSI when the temperature is decreased from 60 to 20 °C, while about a 15-fold increase was obtained for TMHA−TFSI containing 1 M LiTFSI salt in the same temperature range.

The activation energies for the dynamic viscosities were evaluated from the logarithmic form of the Arrhenius equation:

$$\eta = \mathrm{A}\exp(\mathrm{E}_\eta/\mathrm{RT}) \tag{3}$$

E_η is the energy barrier hindering the ions to move past each other. Seen from Figure 3c, the temperature dependence of the dynamic viscosities is well-fit by the Arrhenius model over the temperature range of this study. Slight curvature can be observed in the ln η vs $1/T$ at low temperatures, which implies that the viscosity can be well-described by the Volgel−Tamman−Fulcher (VTF) equation,[35,36]

$$\eta = \mathrm{AT}^{1/2}\exp[\mathrm{B}/(\mathrm{T} - \mathrm{T}_0)] \tag{4}$$

where A is a constant, B is akin to an activation energy, and T_0 is identified as the ideal glass transition temperature.

The value of E_η was calculated from the slope of each plot in Figure 3c. E_η was obtained to be 38.6, 39.1, 45.3, and 53.8 kJ/mol for the ionic liquid containing 0, 0.25, 0.5, and 1.0 M LiTFSI salt, respectively. The uncertainties in the values of E_η were estimated to be less than 1%. The increasing activation energy for dynamic viscosities with increasing LiTFSI concentration is ascribed to the stronger interactions in the RTIL. The larger is E_η, the harder it is for the ions to move past each other. In this sense, the ionic electrolyte containing more LiTFSI salt thus has a stronger association between cations and anions.

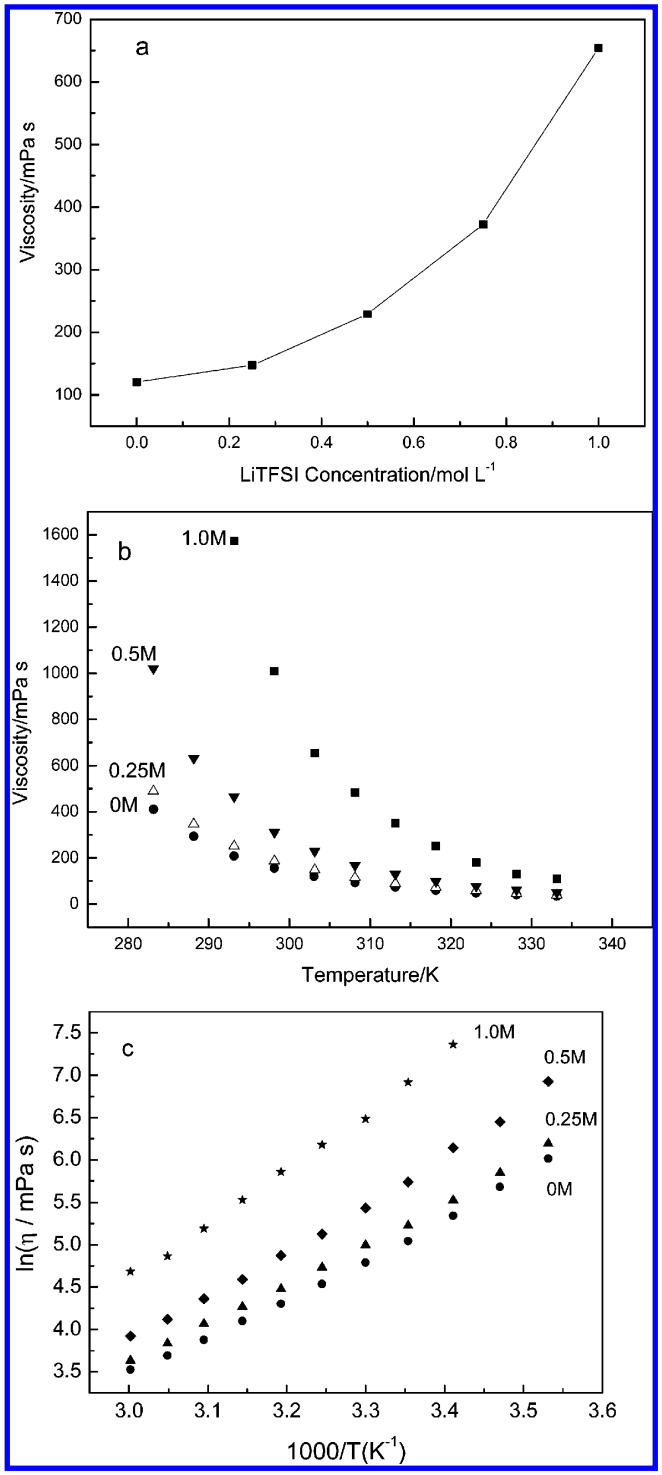

Figure 3. (a) Variation of the viscosity of TMHA−TFSI with LiTFSI concentration at 30 °C, (b) variation of the viscosity of TMHA−TFSI with temperature and differing concentrations of LiTFSI, and (c) Arrhenius plot between the dynamic viscosity and 1/*T*.

Conductivity variation with temperature for TMHA−TFSI containing differing concentrations of LiTFSI salt is displayed in Figure 4a. At room temperature (30 °C), 14.1×10^{-4} S cm^{-1} was measured for the pure TMHA−TFSI ionic liquid. Lithium salt addition decreased the conductivity. Addition of 1 M LiTFSI salt brought the conductivity down to 2.52×10^{-4} S cm^{-1} at the same temperature. The conductivity variation with Li salt concentration is in agreement with the change in the viscosity and indicates that strong interactions exist between ions within the ionic electrolyte.

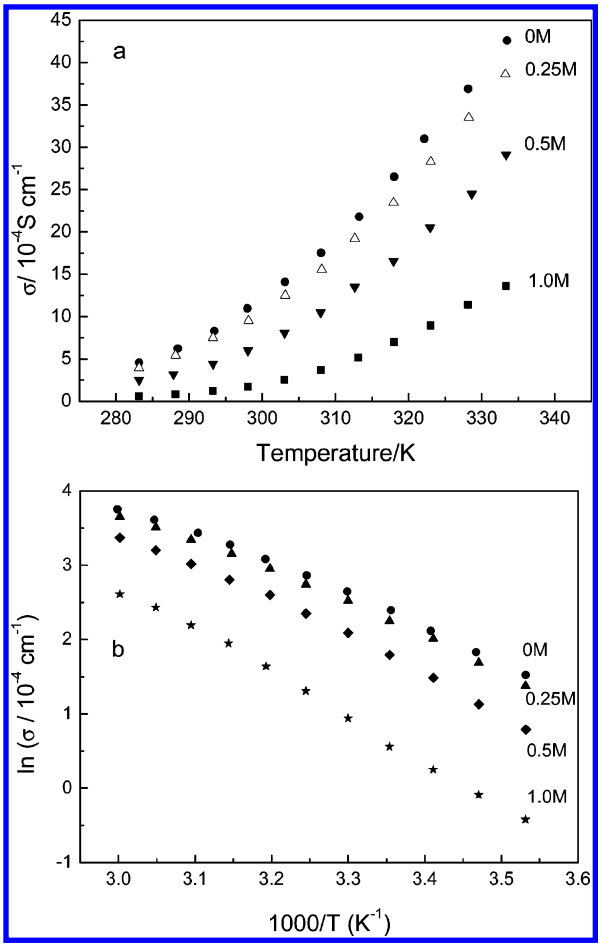

Figure 4. (a) Variation of the conductivity of TMHA−TFSI with temperature and differing concentrations of LiTFSI salt and (b) Arrhenius plot between the conductivity and 1/*T*.

The temperature dependence of conductivity for the ionic solution containing different concentrations of LiTFSI salt obeys the Arrhenius equation,

$$\sigma = A \exp(-E_\sigma/RT) \qquad (5)$$

The Arrhennius plots between conductivity and 1/*T* are shown in Figure 4b. Slighly downward curvature reflects Vogel−Tamman−Fulcher behavior, $\sigma = AT^{1/2} \exp[-B/(T - T_0)]$. The conductivity activation energies determined from the Arrhenius fits were calculated from the angle of the plots. As a result, activation energies of 35.1, 35.8, 39.7, and 50.5 kJ/mol were obtained for the TMHA−TFSI ionic liquid containing 0, 0.25, 0.5, and 1.0 M LiTFSI salt, respectively.

According to the experimental facts, the dynamic viscosities of the TMHA−TFSI ionic liquid containing different concentrations of LiTFSI salt are in inverse proportion to the magnitude of the conductivity. In addition, the conductivity changes with the temperature at quite the same rate as the inverse viscosity because the conductivity activation energy is close with the viscosity activation energy for the ionic electrolyte with the same composition. Walden's rule[37] ($\lambda\eta$ = constant, where λ is the equivalent conductivity and η is the dynamic viscosity) applies to the TMHA−TFSI ionic liquid containing LiTFSI salt. The ionic conductivity of the ionic electrolyte is thus greatly affected by the dynamic viscosity.

Electrochemical windows of the neat TMHA−TFSI ionic liquid were determined by cyclic voltammetry on different materials, as shown in Figure 5. The electrochemical stability

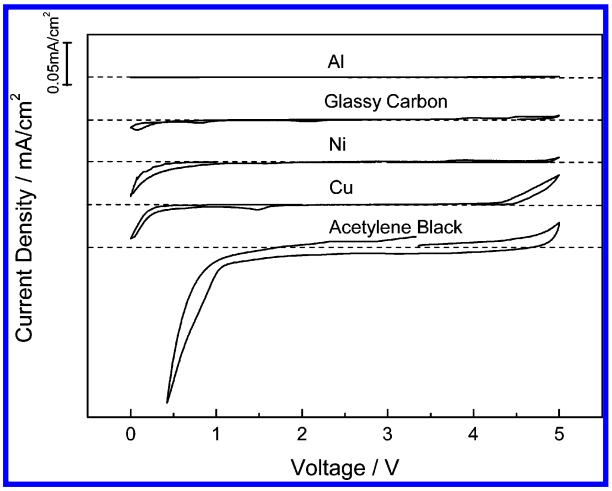

Figure 5. Electrochemical windows of neat TMHA−TFSI ionic liquid on the surfaces of different materials.

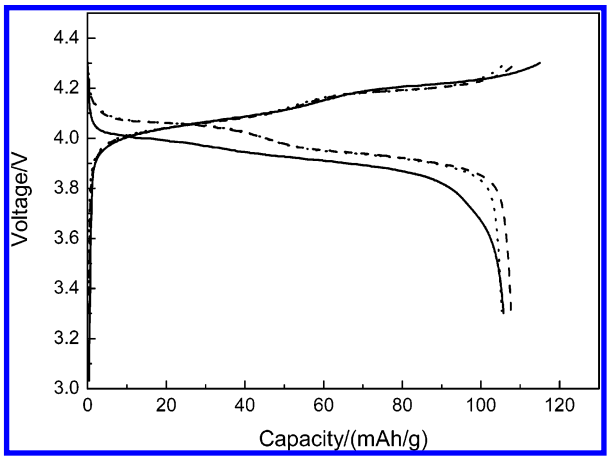

Figure 6. Charge−discharge profiles of a spinel $LiMn_2O_4$ electrode in 1 M LiTFSI/TMHA−TFSI ionic electrolyte at 30 °C. (Solid line, dashed line, and dotted line refer to the first cycle, the fifth cycle, and the tenth cycle, respectively.).

of TMHA−TFSI depends on the electrode materials. On the surface of glassy carbon and Al foil, no obvious reduction and oxidation reaction was detected over the potential range from 0 to 5 V vs Li/Li^+. However, on the surface of Ni foil, Cu foil, and acetylene black, noticeable reduction and oxidation reactions were observed. If we define the potential where reduction reaction occurs on a material as the cathodic limit, we get the cathodic limit of TMHA−TFSI, which becomes negative in the following order: acetylene black > Ni > Cu > glassy carbon ≈ Al. On the other hand, the anodic limit becomes positive in the following order: Cu < acetylene black < Ni < Al ≈ glassy carbon. Since TMHA−TFSI is fairly stable against Al, Al foil is employed as the current collector for the $LiMn_2O_4$ electrode in this study. Acetylene black is used as the conductor for the $LiMn_2O_4$ electrode since no obvious oxidation reaction is observed over the potential from 3 to 4.5 V.

3.2. Temperature Effects on the Electrochemical Behavior of the Li/Ionic Electrolyte/$LiMn_2O_4$ Cell. Charge−discharge profiles of the cell (Li/ionic electrolyte/$LiMn_2O_4$) at a current density of 15 mA/g under room temperature (30 °C) are demonstrated in Figure 6. It is shown that $LiMn_2O_4$ can be effectively cycled in the 1 M LiTFSI/TMHA−TFSI ionic electrolyte. Similar to that of $LiMn_2O_4$ electrode in organic liquid electrolyte, two potential plateaus are observed for each charge or discharge curve, showing the double steps of lithium

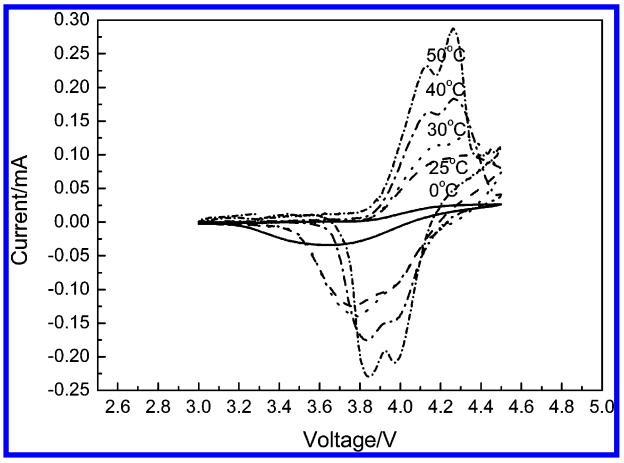

Figure 7. Cyclic voltammograms of the spinel $LiMn_2O_4$ in the ionic electrolyte for the first cycle at a scan rate of 0.05 mV/s under different temperatures.

extraction/insertion from/into $LiMn_2O_4$. Cell performance is almost equivalent to the half-cell using a conventional liquid electrolyte. A discharge capacity of 108.2 mA h/g is obtained with 91.4% coulombic efficiency in the first cycle. This result is quite consistent with that of $LiMn_2O_4$ in a LiCl-saturated $AlCl_3$−EMIC melt reported by Fung and Zhou[20] and compares well with that of $LiMn_2O_4$ in 1 M $LiBF_4$/DMFP−BF_4 ionic electrolyte reported by Caja et al.[38] After 10 electrochemical cycles, no obvious capacity loss was observed, showing the satisfactory cycleability of the $LiMn_2O_4$ cathode in the ionic electrolyte.

Since temperature greatly influences the physiochemical properties of the ionic electrolyte including density, viscosity, and conductivity, etc., the electrochemical performance of the spinel $LiMn_2O_4$ in the ionic electrolyte should also be clearly temperature-dependent. Though the melting point of 14.1 °C for the ionic electrolyte was obtained in Figure 1, the freezing point is well below 0 °C. This is because ionic liquid is prone to supercooling. This phenomenon has been reported in the literature for different ionic liquids.[39,40] Supercooling allows the determination of the $LiMn_2O_4$ cathode properties in the ionic electrolyte at a temperature even lower than 0 °C.

Figure 7 shows the first cyclic voltammograms cycle of $LiMn_2O_4$ electrode in the ionic electrolyte at a scan rate of 0.05 mV/s under different temperatures. All the electrodes subject to cyclic voltammetry (CV) measurements are the same in electrode area and thickness and thus contain the same amount of active materials. This enables the comparison between different diagrams obtained under different temperatures. At low temperature (0 °C), the anodic peak current (i_{pa}) and the anodic peak current (i_{pc}) were very small and no peak split was observed. The large separation between anodic and cathodic potentials shows a serious voltage hysteresis. With increasing temperature, the anodic and cathodic peak currents were increased, indicating the electrode reaction was intensified. The split of anodic and cathodic peaks appears at temperatures above 30 °C, showing the double steps of lithium extraction/insertion from/into the tetrahedral site of the $LiMn_2O_4$ lattice. The growing peak intensity and the approaching of potential separation between the anodic and the corresponding cathodic peaks at elevated temperature reveal that lithium extraction/insertion reaction is facilitated by an increase of temperature.

Figure 8 shows the charge−discharge profiles obtained with the $LiMn_2O_4$ electrode in the ionic electrolyte at a rate of 15 mA/g under various temperatures in the first cycle. On one hand, the charge capacity of the $LiMn_2O_4$ electrode monotonically

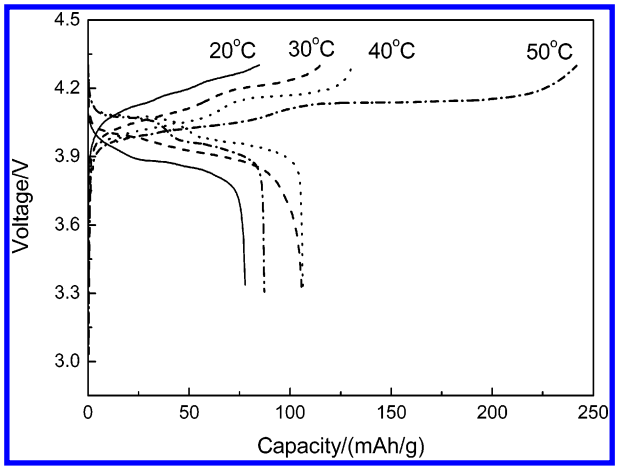

Figure 8. Charge−discharge profiles of the spinel $LiMn_2O_4$ electrode in the ionic electrolyte under different temperatures.

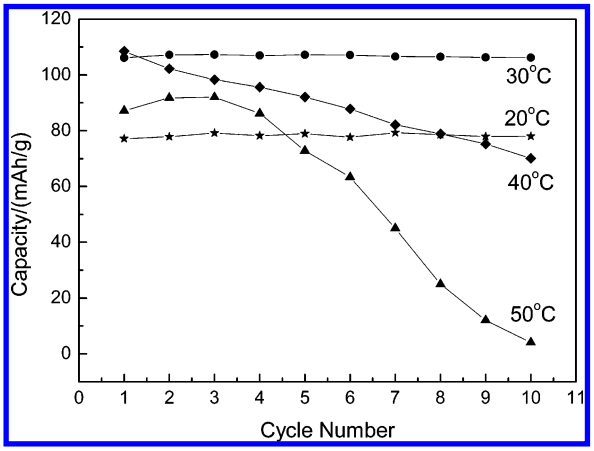

Figure 9. Cycleability of the $LiMn_2O_4$ cathode in 1 M LiTFSI/TMHA−TFSI ionic electrolyte under different temperatures.

increases with increasing temperature. At a temperature of 20 °C, a charge capacity of only 88.4 mA h/g was obtained with a discharge capacity of 77.5 mA h/g. Reversible capacity cannot attain a satisfactory value under this temperature. On the other hand, at an elevated temperature of 50 °C, a charge capacity of 240 mA h/g was obtained. The discharge capacity, however, was only 90.1 mA h/g, resulting in 37.5% coulombic efficiency. An optimum operating temperature of about 30 °C was obtained in terms of reversible capacity and coulombic efficiency in the first cycle.

Figure 9 shows the cycling behavior of the $LiMn_2O_4$ electrode in the ionic electrolyte under different temperatures. Satisfactory cycleability is obtained at 20−30 °C during the initial 10 cycles. When the cell temperature is higher than 40 °C, discharge capacity of the electrode fades rapidly with electrochemical cycles. At a temperature of 50 °C, the spinel $LiMn_2O_4$ electrode lost almost all of its initial capacity after 10 electrochemical cycles.

3.3. Mechanisms Concerning the Temperature Effects of the Spinel $LiMn_2O_4$ Electrode in 1 M LiTFSI/TMHA−TFSI Ionic Electrolyte. Electrochemical impedance spectroscopy (EIS) is a powerful tool for studying lithium ion cells including internal resistance, interfacial phenomenon between electrode and electrolyte, failure mechanism, and so on.[41−43] The EIS technique provides kinetic information of the intercalation compound and allows the resolution of various physical processes. The electrochemical process of the spinel $LiMn_2O_4$ cathode in the ionic electrolyte consists of several steps. That is, Li ion diffusion in the electrolyte, electron insertion/extraction

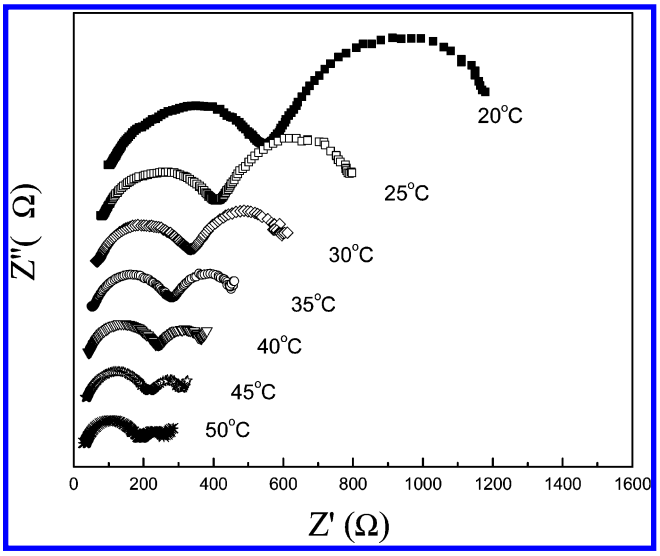

Figure 10. Nyquist plots of spinel $LiMn_2O_4$ measured in ionic electrolyte at a potential of 3.94 V under different temperatures.

into/from the solid phase, charge transfer at the electrode/electrolyte interface, and diffusion of lithium within the $LiMn_2O_4$ electrode. Various models have been suggested relating the impedance responses of porous electrodes with the physical processes. The high-frequency semicircle, intermediate semicircle, and the sloping line in the low frequencies are generally accepted attributes of the Li^+ migration at the electrode surface, interfacial charge-transfer process, and lithium diffusion within the solid phase, respectively.[44−46] Some auththors[47] proposed that the high-frequency semicircle was ascribed to the particle/particle contact resistance or the electrode/current collector interface, while the medium-to-low-frequency semicircle was related to the incorporation of lithium ions into the solid phase. Other authors[48] have attributed the high-to-medium-frequency semicircle to interfacial charge-transfer process and the medium-to-low-frequency semicircle to the absorption of lithium ions into the electrode.

Typical Nyquist plots of the $LiMn_2O_4$ cathode obtained in 1 M LiTFSI/TMHA−TFSI ionic electrolyte under different temperatures at 3.94 V are shown in Figure 10. Each diagram shows two semicircles. The high-frequency limit refers to the bulk electrolyte resistance. The high-to-medium-frequency semicircle, which did not show obvious evolution with the electrode potential, is ascribed to the contact resistance at the oxide particle/current collector interface or oxide particle/particle interface.[47,49,50] The semicircle in the middle frequency region is attributed to the charge-transfer process at the interface of the $LiMn_2O_4$/ionic electrolyte.[49,50] The sloping line at low frequencies is attribute to a semiinfinite diffusion of lithium ions in the $LiMn_2O_4$ electrode, which is not clearly distinguishable at temperatures below 30 °C.

Under low temperature, the large electrolyte resistance comes from the high electrolyte viscosity as discussed above. The high contact resistance at the oxide particle/current collector interface or oxide particle/particle interface and the large charge transfer at the electrode/electrolyte interface are probably associated with the poor wettability of the electrolyte with the active electrode particle surface. The total internal resistance obtained is several times larger than that in the traditional organic electrolyte. It is known that the bulk electrolyte resistance and contact resistance cause the ohmic potential drop, while the charge-transfer resistance may control the rate of lithium insertion. The high internal resistance is thus an important factor responsible for

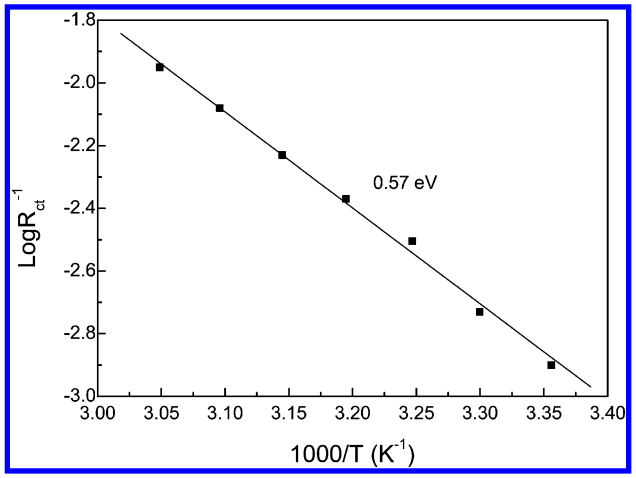

Figure 11. Temperature dependence of charge-transfer resistance at the interface between $LiMn_2O_4$ and ionic electrolyte.

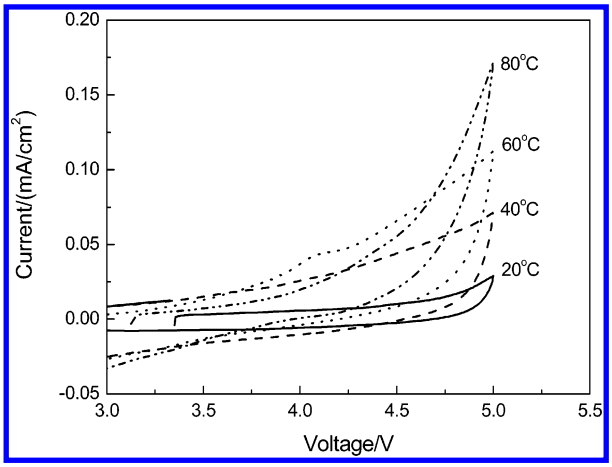

Figure 12. Oxidation behavior of TMHA−TFSI on the surface of acetylene black under different temperatures.

the poor electrochemical performance of $LiMn_2O_4$ electrode in the ionic electrolyte under low temperature.[51−53]

With increasing temperature, the high-frequency limit shifts in the negative direction on the real axis reflecting the decrease of electrolyte resistance. Shrinkage of the first arc in the high-frequency region shows the decrease of the contact resistance at the oxide particle/current collector interface or oxide particle/particle interface. Shrinkage of the second semicircle in the middle frequency region exhibits the decrease of charge-transfer resistance at the interface between the $LiMn_2O_4$ electrode and the ionic electrolyte. All the reaction steps of the lithium intercalation are thermally activated processes.

The rate-controlling process can be distinguished from various steps by the variation of the reaction rates with temperature. Among all the different internal resistances, the charge-transfer resistance at the electrolyte/electrode interface is strongly dependent on temperature (and also on the electrode potential). The transfer of lithium ions through the electrolyte/electrode interface is therefore a rate-controlling process of the lithium intercalation into the $LiMn_2O_4$ electrode. According to the Arrhenius expression of a thermally activated process, the charge-transfer resistance (R_{ct}) can be written as

$$R_{ct} = A \exp(E_a/RT) \quad (6)$$

or

$$1/R_{ct} = A' \exp(-E_a/RT) \quad (7)$$

where A is the preexponential factor ($A' = 1/A$), T refers to the absolute temperature, and E_a represents the apparent activation energy of lithium ion transfer through the electrolyte/electrode interface. The activation energy for the interfacial Li ion transfer at the electrode potential of 3.94 V was evaluated from the temperature dependence of the charge-transfer resistances as shown in Figure 11. Good linearity of the Arrhennius plot between $1/R_{ct}$ and $1/T$ was observed. The apparent activation energy for the charge-transfer process was calculated from the angle of the plot. As a result, a value of 0.57 ± 0.05 eV was obtained. This value of activation energy is considerably large in comparison with the activation energy for lithium ion conduction through positive active material of $LiCoO_2$[54] (0.3 eV) and $LiFePO_4$[55] (ca. 0.2 eV). Compared with the reported activation energy of lithium ion transfer obtained to be about 0.5 eV at the interface of $LiMn_2O_4$[56] in a viscous organic electrolyte, 1 M $LiClO_4$−PC electrolyte, this value of activation energy is also higher. For $LiMn_2O_4$ in the ionic electrolyte, poor wettabilty of the electrolyte with the electrode, high electrolyte viscosity and the formation of close contact ion pairs between Li^+ and TFSI, all the factors decrease Li^+ mobility and contribute to the large activation energy. The large activation energy implies that a high energy barrier exists, hindering lithium ion transfer at the interface between $LiMn_2O_4$ electrode and the ionic electrolyte. A low temperature hinders lithium intercalation due to the high activation energy.

To understand the electrochemical decay of the Li/ionic electrolyte/$LiMn_2O_4$ cell at elevated temperature, we examined the stability of TMHA−TFSI on the electrode conductor (acetylene black) under different temperatures. As shown in Figure 12, increasing temperature promotes the oxidation reaction of TMHA−TFSI on the acetylene black. At elevated temperature, the onset of oxidation potential becomes negative and the intensity of oxidation current gets stronger. The electrolyte may be oxidized at a very positive operation potential on the surface $LiMn_2O_4$ electrode, especially when an undesirable catalytic activity of $LiMn_2O_4$ occurs.[57] Seen from Figure 8, the charge capacity was greatly increased by raising the temperature (up to 50 °C), which indicates strong side reactions are involved in the anodic process. Anodic oxidation of electrolyte is the main side reaction form leading to the high charge capacity. From this viewpoint, the strong side reactions during the anodic process account for the decrease of Coulombic efficiency with increasing temperature. Oxidation reaction of electrolyte is known for bringing about the electrochemical deterioration of $LiMn_2O_4$ electrode in traditional organic electrolytes[58] and promoting the dissolution of $LiMn_2O_4$ active material during the electrochemical process at elevated temperature.[59] This effect leads to capacity fading of the electrode with electrochemical cycles.

Figure 13 shows the X-ray diffraction profiles of the original $LiMn_2O_4$ electrode and the $LiMn_2O_4$ electrode having cycled for 10 electrochemical cycles in 1 M LiTFSI/EC + DEC organic electrolyte under room temperature and in 1 M LiTFSI/TMHA−TFSI ionic electrolyte at 50 °C, respectively. After 10 electrochemical cycles in the conventional organic electrolyte, the XRD pattern of $LiMn_2O_4$ electrode is quite consistent with that obtained from the original $LiMn_2O_4$ electrode. Good structural reversibility of the $LiMn_2O_4$ electrode is obtained. After being cycled in the ionic electrolyte under high temperature, however, many new peaks designated by asterisks appeared in the XRD pattern. The appearance of these new peaks suggests the formation of a new phase within the electrode, which may be

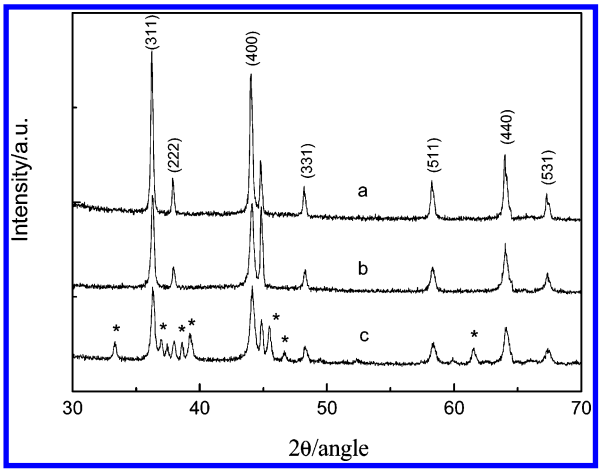

Figure 13. XRD patterns of (a) the original $LiMn_2O_4$ electrode, (b) the $LiMn_2O_4$ electrode having cycled 10 electrochemical cycles in 1 M LiTFSI/EC + DEC electrolyte under room temperature, and (c) in 1 M LiTFSI/TMHA−TFSI electrolyte at 50 °C.

due to TMHA cation intercalation. Of course, Jahn−Teller (J−T) cooperative distortion by a cubic to orthorhombic transition is one of the most important factors contributing to capacity fading.[60,61] In a 4 V $LiMn_2O_4$ cell, Jahn−Teller distortion occurs at low electrode potential, resulting in a phase transition from the cubic phase to the tetragonal phase, which leads to the loss of the electroactive materials, poor electronic contact, and results in capacity fading. With increasing lithium concentration or at high lithium ion insertion rate, Jahn−Teller distortion becomes important, especially at the surface of the $LiMn_2O_4$ particle. A detailed mechanism for the Jahn−Teller distortion of the $LiMn_2O_4$ electrode in an ionic electrolyte needs thorough investigation. Anyway, the irreversible structural conversion of the $LiMn_2O_4$ electrode can, in another sense, explain the electrochemical decay of $LiMn_2O_4$ at elevated temperature.

IV. Conclusion

Although with a wide liquid-phase temperature range, the physiochemical properties of ionic electrolyte solution are strongly temperature-dependent. Electrochemical properties of a spinel $LiMn_2O_4$ cathode in the ionic electrolyte were strongly influenced by the variation of temperature. An optimum operating temperature of ca. 30 °C was obtained for the cell using 1 M LiTFSI/TMHA−TFSI ionic electrolyte in terms of reversible capacity, coulombic efficiency, and the cycleability. The cell impedance, including the bulk electrolyte resistance, the contact resistance between the oxide particle and current collector, and the interface resistance at the electrode and the electrolyte, is obviously high in comparison with the cell using conventional organic electrolyte. Lithium ion transfer through the electrode/ionic electrolyte interface is a rate-controlling step of the lithium intercalation into the $LiMn_2O_4$ electrode. A large activation energy for the lithium-transfer process implies that a high-energy barrier exists hindering lithium ion transfer at the $LiMn_2O_4$/ionic electrolyte interface. The high cell impedance and the large activation energy for lithium ion transfer at the electrode/electrolyte interface account for the low electrode capacity under low temperature. Strong side reactions during charge, especially oxidation reaction of TMHA−TFSI on acetylene black, results in the decrease of coulombic efficiency for the $LiMn_2O_4$ electrode in the ionic electrolyte at elevated temperature. Electrolyte oxidation also promotes dissolution of the spinel $LiMn_2O_4$ active material and thus leads to capacity fading of the electrode with electrochemical cycles. The irreversible structural conversion of $LiMn_2O_4$, possibly associated with the formation of TMHA intercalated compounds or the occurrence of Jahn−Teller distortion, is the other factor leading to the capacity fading of the $LiMn_2O_4$ electrode. To widen the operating temperature of lithium (ion) batteries by using ionic electrolyte, satisfactory solution must be taken to avoid the temperature effects.

Acknowledgment. The authors are greatly indebted to the funding of Natural Science Foundation of China (NSFC, Contract No. 20273019) and the funding of the young researcher's program of Henan Province (Grant No. 04120001100), China.

References and Notes

(1) Demberelnyamba, D.; Shin, B. K.; Lee, H. *Chem. Commun.* **2002**, 1538.
(2) Welton, T. *Chem. Rev.* **1999**, *99*, 2071.
(3) Marsh, K. N.; Boxall, J. A.; Lichtenthaler, R. *Fluid Phase Equilib.* **2004**, *219*, 93.
(4) Visser, A. E.; Rogers, R. D. *J. Solid State Chem.* **2003**, *171*, 109.
(5) Earle, M. J.; Seddon, K. R. *Pure Appl. Chem.* **2000**, *72*, 1391.
(6) Sato, T.; Masuda, G.; Takagi, K. *Electrochim. Acta* **2004**, *49*, 3603.
(7) Ue, M.; Takeda, M.; Toriumi, A.; Kominato, A.; Hagiwara, R.; Ito, Y. *J. Electrochem. Soc.* **2003**, *150*, A499.
(8) Papageorgiou, N.; Athanassov, Y.; Armand, M.; Bonhote, P.; Pettersson, H.; Azam, A.; Gratzel, M. *J. Electrochem. Soc.* **1996**, *143*, 3099.
(9) Matsui, H.; Okada, K.; Kawashima, T.; Ezure, T.; Tanabe, N.; Kawano, R.; Watanabe, M. *J. Photochem. Photobiol., A* **2004**, *164*, 129.
(10) Hu, Y.; Li, H.; Huang, X.; Chen, L. *Electrochem. Commun.* **2004**, *6*, 28.
(11) Sato, T.; Maruo, T.; Marukane, S.; Takagi, K. *J. Power Sources* **2004**, *138*, 253.
(12) Fuller, J.; Carlin, R. T.; Osteryoung, R. A. *J. Electrochem. Soc.* **1997**, *144*, 3881.
(13) Noda, A.; Hayamizu, K.; Watanabe, M. *J. Phys. Chem. B* **2001**, *105*, 4603.
(14) Shin, J.-H.; Henderson, W. A.; Passerini, S. *Electrochem. Commun.* **2003**, *5*, 1016.
(15) Holzapfel, M.; Jostb, C.; Novak, P. *Chem. Commun.* **2004**, 2098.
(16) Wilkes, J. S.; Zaworotko, M. J. *J. Chem. Soc., Chem. Commun* **1992**, 965.
(17) Fung, Y. S.; Zhou, R. Q. *J. Power Sources* **1999**, *81*, 891.
(18) Nakagawa, H.; Izuchi, S.; Kuwana, K.; Nukuda, T.; Aihara, Y. *J. Electrochem. Soc.* **2003**, *150*, A695.
(19) Garcia, B.; Lavallee, S.; Perron, G.; Michot, C.; Armand, M. *Electrochim. Acta* **2004**, *49*, 4583.
(20) Fung, Y. S.; Zhou, R. *Electrochemistry* **1999**, *67*, 713.
(21) Koch, V. R.; Nanjundiah, C.; Appetecchi, G. B.; Scrosati, B. *J. Electrochem. Soc.* **1995**, *142*, 116.
(22) Sun, J.; Forsyth, M.; MacFarlane, D. R. *J. Phys. Chem. B* **1998**, *102*, 8858.
(23) MacFarlane, D. R.; Meakin, P.; Sun, J.; Amini, N.; Forsyth, M. *J. Phys. Chem. B* **1999**, *103*, 4164.
(24) Sakaebe, H.; Matsumoto, H. *Electrochem. Commun.* **2003**, *5*, 594.
(25) Howlett, P. C.; MacFarlane, D. R.; Hollenkamp, A. F. *Electrochem. Solid-State Lett.* **2004**, *7*, A97.
(26) Egashira, M.; Okada, S.; Yamaki, J.; Dri, D. A.; Bonadies, F.; Scrosati, B. *J. Power Sources* **2004**, *138*, 240.
(27) Okoturo, O. O.; VanderNoot, T. J. *J. Electroanal. Chem.* **2004**, *568*, 167.
(28) Shobukawa, H.; Tokuda, H.; Tabata, S.−I.; Watanabe, M. *Electrochim. Acta* **2004**, *50*, 1.
(29) Katayama, Y.; Yukumoto, M.; Miura, T. *Elelctrochem. Solid-State Lett.* **2003**, *6*, A96.
(30) Wang, J.; Tian, Y.; Zhao, Y.; Zhuo, K. *Green Chem.* **2003**, *5*, 618.
(31) Soon, J. Y.; H. Lee, H.; Wang, Y. Y.; Wan, C. C. *J. Power Sources* **2002**, *111*, 255.
(32) McFarlane, D. R.; Sun, J.; Golding, J.; Meakin, P.; Forsyth, M. *Electrochim. Acta* **2000**, *45*, 1271.
(33) Marsh, K. N.; Boxall, J. A.; Lichtenthaler, R. *Fluid Phase Equilib.* **2004**, *21*, 993.
(34) Xu, W.; Cooper, E. I.; Angell, C. A. *J. Phys. Chem. B* **2003**, *107*, 6170.
(35) Vogel, H. *Phys. Z.* **1921**, *22*, 645; Tamman, G.; Hesse, W. *Z. Anorg. Allg. Chem.* **1926**, *156*, 245. Fulcher, G. S. *J. Am. Ceram. Soc.* **1925**, *8*, 339.

(36) Carpio, R. A.; King, L. A.; Lindstram, R. E.; Nardi, J. C.; Hussey, C. L. *J. Electrochem. Soc.* **1979**, *126*, 1644. Sanders, J. R.; Ward, E. H.; Hussey, C. L. *J. Electrochem. Soc.* **1986**, *133*, 325.
(37) Walden, P. *Z. Phys. Chem.* **1906**, *55*, 207, 246.
(38) Caja, J.; Dunstan, T. D.; Ryan, D. M.; Katovic, V. *Molten Salts XII*; Electrochemical Society: Pennington, NJ, 2000; p 150.
(39) Wilkes, J. S. *J. Mol. Catal. A: Chem.* **2004**, *214*, 11.
(40) Zhou, Z. B.; Takeda, M.; Ue, M. *J. Fluorine Chem.* **2004**, *125*, 471
(41) Fan, J.; Fedkiw, P. S. *J. Electrochem. Soc.* **1997**, *144*, 399.
(42) Gaberscek, M.; Pejovnik, S. *Electrochim. Acta* **1996**, *41*, 1137.
(43) Koksbang, R.; Olsen, I. I.; Tonder, P. E.; Knudsen, N.; Fauteux, D. *J. Appl. Electrochem.* **1991**, *21*, 301.
(44) Thomas, M. G. S. R.; Bruce, P. G.; Goodenough, J. B. *J. Electrochem. Soc.* **1985**, *132*, 1521.
(45) Aurbach, D.; Gamolsky, K.; Markovsky, B.; Salitra, G.; Gofer, Y.; Heider, U.; Oesten, R.; Schmidt, M. *J. Electrochem. Soc.* **2000**, *147*, 1322.
(46) Meyers, J. P.; Doyle, M.; Darling, R. M.; Newman, J. *J. Electrochem. Soc.* **2000**, *147*, 2930.
(47) Choi, Y. M.; Pyun, S. I.; Bae, J. S.; Moon, S. I. *J. Power Sources* **1995**, *56*, 25. Chang, Y.-C.; Sohn, H. J. *J. Electrochem. Soc.* **2000**, *147*, 50.
(48) Li, H.; Lu, Z.; Huang, H.; Huang, X.; Chen, L. *Ionics* **1996**, *2*, 259.
(49) Hjelm, A.-K.; Lindbergh, G. *Electrochim. Acta* **2002**, *47*, 1747.
(50) Choi, Y.-M.; Pyun, S.-I.; Moon, S.-I. *Solid State Ionics* **1996**, *89*, 43.
(51) Takahashi, M.; Tobishima, S.; Tabei, K.; Sakurai, Y. *Solid State Ionics* **2002**, *148*, 283.
(52) Iriyama, Y.; Kurita, H.; Yamada, I.; T. Abe Ogumi, Z. *J. Power Sources* **2004**, *137*, 111.
(53) Fan, J.; Fedkiw, P.-S. *J. Power Sources* **1998**, *72*, 165.
(54) Nakamura, K.; Ohno, H.; Okamura, K.; Michihiro, Y.; Nakabayashi, I.; Kanashiro, T. *Solid State Ionics* **2000**, *135*, 143.
(55) Takahashi, M.; Tobishima, S.; Tabei, K.; Sakurai, Y. *Solid State Ionics* **2002**, *148*, 283.
(56) Kim, S.-W.; Pyun, S.-I. *J. Electroanal. Chem.* **2002**, *528*, 114.
(57) Kanamura, K.; Toriyama, S.; Shiraishi, S.; Takehara, Z. *J. Electrochem. Soc.* **1996**, *143*, 2548.
(58) MacNeil, D. D.; Lu, Z.; Chen, Z.; Dahn, J. R. *J. Power Sources* **2002**, *108*, 8.
(59) Besenhard, J. O. *Handbook of Battery Materials*; Wiley-VCH: New York, 1999; p 311.
(60) Thackeray, M. M.; Shao-Horn, Y.; Kahaian, A. J.; Kelper, K. D.; Skinner, E.; Vaughey, J. T.; Hackney, S. A. *Electrochem. Solid-State Lett.* **1998**, *1*, 7.
(61) Gummow, R. J.; de Kock, A.; Thackeray, M. M. *Solid State Ionics* **1994**, *69*, 59.